ACS Catalysis

Research Article

pubs.acs.org/acscatalysis

A Highly Active "NiO-on-Au" Surface Architecture for CO Oxidation

Xuejun Xu, Qiang Fu,* Xiaoguang Guo, and Xinhe Bao

State Key Laboratory of Catalysis, Dalian Institute of Chemical Physics, Chinese Academy of Sciences, Dalian 116023, China

ABSTRACT: Supported Au−Ni nanocatalysts consisting of Au nanoparticles decorated with Ni/NiO nanostructures were synthesized using a two-step method and characterized by X-ray diffraction, transmission electron microscopy, X-ray photoelectron spectroscopy, and X-ray absorption spectroscopy. The structural characterization indicates that a small part of surface Ni atoms can diffuse into Au cores upon reduction at 600 °C, while the alloyed Ni atoms segregate onto the Au nanoparticle surfaces when oxidizing at a similar temperature. The inward and outward diffusion of Ni atoms at Au surfaces are reversible with response to cycled reduction and oxidation treatments. CO oxidation reactions over the Au−Ni catalysts suggest that Au nanoparticles decorated with highly dispersed NiO nanopatches are the active surface architecture. Optimum activity has been observed by maximizing the density of boundaries between NiO patches and Au surfaces, which can be achieved through suitable redox pretreatments of the Au−Ni catalysts. NiO surface structures in the "NiO-on-Au" inverse catalysts not only enhance Au-catalyzed CO oxidation performance but also prevent sintering of Au nanoparticles at elevated temperatures. Similar high activity for the CO oxidation has been observed in the "CoO_x-on-Au" and "FeO_x-on-Au" inverse catalysts.

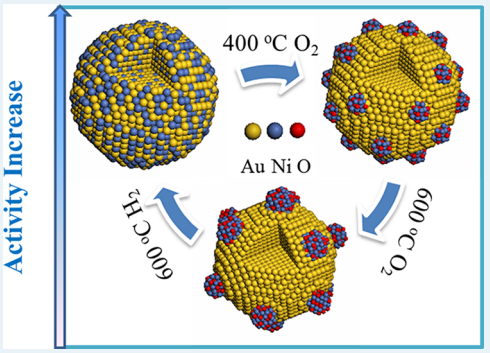

KEYWORDS: *inverse catalysts, Au catalysis, CO oxidation, NiO, redox treatment*

1. INTRODUCTION

Supported Au nanoparticles (NPs) with sizes smaller than 5 nm exhibit remarkable catalytic performance in many oxidation and hydrogenation reactions.[1−4] It has been shown that the catalytic activity of Au catalysts is strongly dependent on the nature of supports.[5−7] Au NPs dispersed on reducible oxides such as TiO_2, Fe_2O_3, and CeO_2 may have smaller sizes and present high catalytic performance compared to those supported on inert oxides, e.g., SiO_2 and Al_2O_3.[8] The strong metal−support interaction between Au NPs and the reducible oxides helps to stabilize small Au NPs and, moreover, produces active sites at the Au/oxide interfaces.[9−13] Furthermore, electron transfer between the metal and the oxide support charges the Au NPs and enhances their activity as well.[14,15] Alternatively, the electronic structure and catalytic property of Au NPs can be modulated by another metal with rational design of their surface structure. For instance, supported Au−Pt,[16−18] Au−Pd,[19−22] and Au−Ag[23,24] bimetallic NPs with heterostructure, core−shell, or alloy nanostructures perform better than their parent metals in CO oxidation, oxygen reduction reaction, formic acid eletrooxidation, alcohol oxidation, and acetoxylation of ethylene.

Recently, inverse catalysts consisting of oxide nanostructures decorated on metal surfaces have attracted intensive attention.[25−30] Due to the strong interaction between transition metal oxides (TMOs) and noble metals (NMs), the supported TMOs are often two-dimensional (2D) in their morphology and metastable in the chemical state. The formed TMO/NM interfaces help to stabilize coordinatively unsaturated (CUS) metal cations exposed at the edges of 2D TMO nanoislands, which are highly active in many reactions.[29,30] In our previous works, the TMO-on-Pt (TM = Fe, Co, and Ni) catalysts have been constructed and were applied in low temperature catalytic oxidation reactions.[31−34] It has been demonstrated that surface TMO nanolayers confined on Pt surfaces significantly enhance the catalytic performance of Pt. Considering that 2D TMO nanostructures can be stabilized by Au surfaces,[35] the "TMO-on-NM" structural configuration may be further applied to Au-based catalytic systems. In the present work, we show that "NiO-on-Au" surface architecture can be constructed in Au−Ni bicomponent catalysts. The NiO-on-Au surface structures are highly active in CO oxidation such that the extraordinary performance is not critically dependent on Au particle size and support.

2. EXPERIMENTAL SECTION

Au−Ni/SiO_2 catalysts were prepared using a two-step synthetic method, similar to that used for preparation of Pt−Fe/SiO_2 catalysts.[31] Briefly, 1 g of commercial silica (Qingdao Ocean Chemical Company) was functionalized with APTES (H_2N-$(CH_2)_3Si(OEt)_3$). Then, 8.36 mL of $HAuCl_4$ solution (2.5×10^{-2} mol/L) was added to the functionalized SiO_2 support, followed by reduction with $NaBH_4$. After filtration and washing, the resulted Au/SiO_2 powders were mixed with a certain amount of $Ni(NO_3)_2$ solution (0.05 mol/L) at 75 °C, and the Ni^{2+} ions were reduced onto the Au NPs' surfaces using

Received: March 14, 2013
Revised: June 24, 2013
Published: June 27, 2013

   dx.doi.org/10.1021/cs400197t | ACS Catal. 2013, 3, 1810−1818

hydrazine hydrate as reducing agents.[36] The nominal Au loadings in all catalysts were fixed at 4 wt %, while those of Ni can be varied. For the preparation of Au−Fe/SiO_2 and Au−Co/SiO_2 catalysts, a similar process was applied, but replacing $Ni(NO_3)_2$ with $Fe(NO_3)_3$ or $Co(NO_3)_2$.

Before activity testing and structure characterization, the as-prepared catalysts were exposed to different gases (O_2, H_2, or Ar) with a flow rate of 30 mL/min and heated at a specific temperature for 2 h. After cooling down to room temperature (RT), the gas stream was switched to the reaction atmosphere (1% CO and 20% O_2 balanced with He) with a flow rate of 50 mL/min and gas hourly space velocity (GHSV) equal to 75 000 $mL{\cdot}g^{-1}{\cdot}h^{-1}$, if not specified. For measurements of specific reaction rates and apparent activation energy, reactions were performed under a kinetic-limiting region by controlling GHSV. The catalytic performance was investigated from RT to 300 °C with a heating rate of 1 °C/min. Gas products were analyzed with a micrgas chromatograph (GC-490) equipped with a 5 Å molecular sieve column and a thermal conductivity detector.

X-ray diffraction (XRD) patterns were collected on a Rigaku D/Max 2500 diffractometer using a Cu Kα (λ = 1.5406 Å) radiation source. X-ray photoelectron spectroscopy (XPS) measurements were performed using a Thermo Scientific ESCALAB 250Xi spectrometer. The XP spectra were obtained with an Al Kα X-ray source, and the passing energy was fixed at 20 eV. The Si 2p peak located at 103.9 eV from the SiO_2 support was used for calibration of binding energies, and the intensity of both Ni 2p and Au 4f spectra has been normalized to that of the Si 2p peak. Transmission electron microscopy (TEM) images were recorded on the FEI Tecnai G2 microscope operated at an acceleration voltage of 120 kV. The actual loading of Au in all samples was determined by washing the samples in aqua regia solution and measuring the Au ion concentrations in the leached solutions by inductively coupled plasma atomic emission spectrometry (ICP-AES; ICPS-8100, Shimadzu). The leaching experiments were also performed using a dilute nitric acid solution (30 mmol/L) to selectively wash Ni species from the samples. Extended X-ray absorption fine structure (EXAFS) was measured at the BL14W1 beamline of the Shanghai Synchrotron Radiation Facility (SSRF). Ni K-edge EXAFS spectra of the catalysts were collected in fluorescence mode. For comparison, those of Ni foil and the standard NiO sample were recorded in transmission mode.

3. RESULTS

3.1. Catalytic Activity for CO Oxidation. The as-prepared Au/SiO_2 and Au−Ni/SiO_2 catalysts were calcined in the air at 600 °C to remove surfactant and then reduced in H_2 at 600 °C for 2 h. After the pretreatments, they were subjected to the CO oxidation test. As shown in Figure 1, the pure Au/SiO_2 catalyst exhibits a U-shape dependence of activity with the reaction temperature and presents the temperature for complete CO conversion (T_{100}) at 250 °C. This catalytic behavior is similar to the previous results.[37−39] It has been documented that CO oxidation over Au NPs occurs via low-temperature and high-temperature reaction mechanisms. In the low-temperature range, CO molecules mainly react with weakly absorbed O_2 or surface hydroxyl groups. An increase in the reaction temperature decreases the coverage of the weakly absorbed oxygen-containing surface species and, consequently, lowers the catalytic activity. In contrast, O_2 can dissociate at the

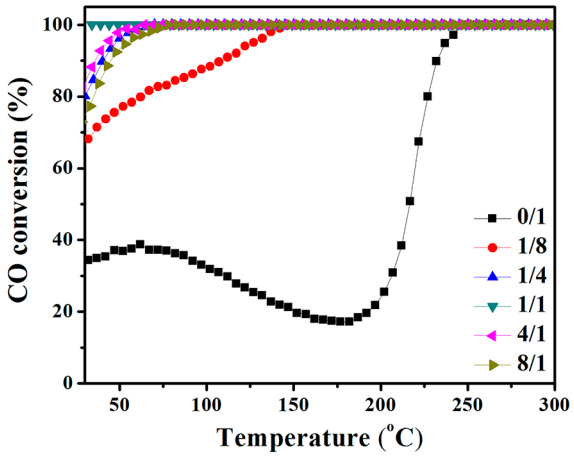

Figure 1. CO conversion light-off curves over Au−Ni/SiO_2 catalysts with different Ni/Au atom ratios.

Au surface in the high temperature region, in which CO oxidation activity shows a normal Arrhenius-type behavior. A U-shape reaction curve is exhibited because of the transition from the low-temperature mechanism to the high-temperature mechanism. The CO oxidation activity of the Au−Ni/SiO_2 catalysts has been improved significantly, showing the promotional effect of the Ni component on the Au-catalyzed reaction. The activity increases when the Ni/Au atom ratio changes from 1:8 to 1:1, while a further increase in the Ni/Au ratio from 1:1 to 8:1 results in a decrease in the activity. Accordingly, an optimum Ni/Au ratio at 1:1 was chosen for all the following studies.

The effect of oxidation treatment on the CO oxidation activity was studied first. The as-prepared Au−Ni/SiO_2 catalyst oxidized at 400 °C also exhibits a U-shape curve and achieves a complete CO conversion at 190 °C (Figure 2A). Oxidation at much higher temperatures results in a much broader valley in its light-off curve. At the same time, the temperature for complete CO conversion shifts to a higher temperature, which almost approaches that of the Au/SiO_2 catalyst. Therefore, it can be concluded that the promotional effect of Ni has been suppressed by the high temperature oxidation treatment.

Next, the Au−Ni/SiO_2 catalyst oxidized at 600 °C was further reduced at various temperatures in H_2, and the influence of the reduction treatment on the reaction was investigated. The reaction results show that the reduced catalysts all present improved CO oxidation activity compared to the Au/SiO_2 catalyst and the oxidized Au−Ni/SiO_2 catalysts (Figure 2B). Particularly, the samples reduced at an intermediate temperature such as 500 and 600 °C present the best performance, in which the CO conversion is nearly 100% between RT and 300 °C.

To further investigate the effect of the redox treatments on the reaction, the Au−Ni/SiO_2 catalysts were treated in alternating H_2 and O_2 atmospheres. The CO oxidation reaction was carried out using a higher GHSV of 120 000 $mL{\cdot}g^{-1}{\cdot}h^{-1}$ in order to see the reactivity difference (Figure 3A). The catalyst oxidized at 600 °C shows a very low activity with a broad valley in its activity curve. The subsequent reduction at 600 °C improves the reaction activity significantly, in which CO conversion is higher than 80% at RT and reaches 100% at 85 °C. With one more oxidation step at 400 °C, the catalyst was also very highly active for CO oxidation. After the second oxidation treatment at 600 °C, however, T_{100} is higher than 200

dx.doi.org/10.1021/cs400197t | ACS Catal. 2013, 3, 1810−1818

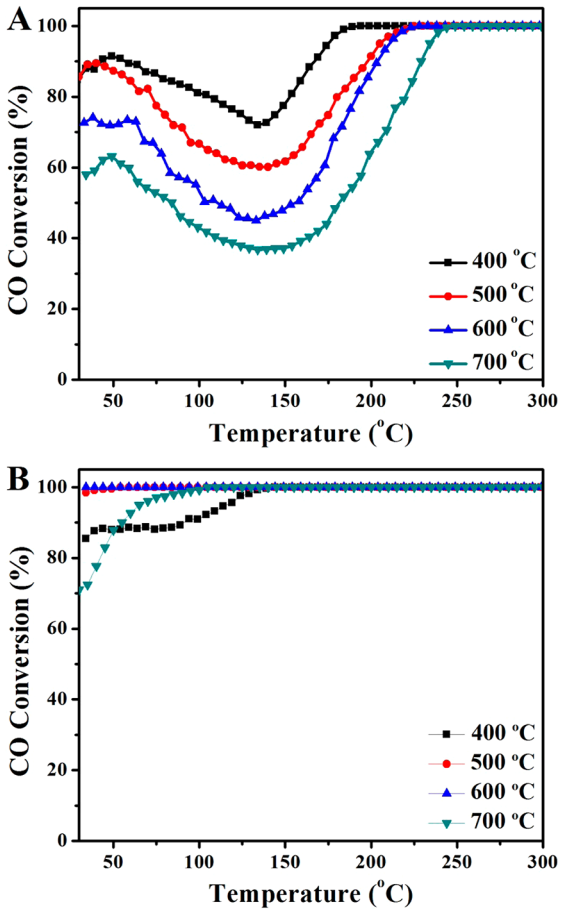

Figure 2. CO conversion light-off curve over Au−Ni/SiO_2 catalysts treated under different conditions: (A) oxidation at different temperatures, (B) reduction at different temperatures.

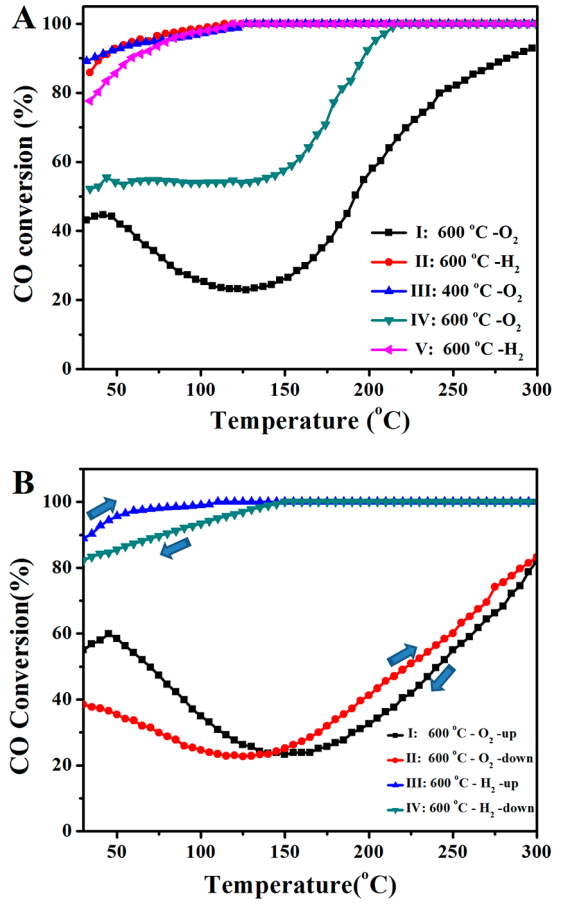

Figure 3. (A) The CO conversion light-off curve over Au−Ni/SiO_2 catalysts subjected to sequential redox treatments. (B) The CO conversion light-off curves with temprature ramped up (I, III) and ramped down (II, IV) over the Au−Ni/SiO_2 catalyst oxidized at 600 °C (I, II) and the Au−Ni/SiO_2 catalyst reduced at 600 °C (III, IV). GHSV = 120 000 mL g^{-1} h^{-1}.

°C. Finally, the CO conversion can resume up to 80% at RT and approach 100% at 100 °C after the second reduction treatment at 600 °C. It should be noted that the reaction activity does not experience big change when ramping down the reaction temperature to RT. Two typical Au−Ni/SiO_2 catalysts, which were subjected to oxidation at 600 °C and reduction at 600 °C, respectively, were tested in the CO oxidation with the temperature ramped up first and then ramped down (Figure 3B). Only a slight decrease in the activity can be observed for the reduced Au−Ni/SiO_2 catalyst in the cooling process. The typical U-shape reaction curve has been observed in the oxidized catalyst upon cooling. The results demonstrate that the active sites have been kept during the cyclic up and down temperature test.

The specific reaction rates at 30 °C of the Au catalyst and the typical Au−Ni catalysts were measured by carrying out the reactions at much higher GHSVs [Table 1]. The pure Au/SiO_2 catalyst has a specific reaction rate of 0.26 mol_{CO} g_{Au}^{-1} h^{-1}. That of the Au−Ni/SiO_2 catalyst reduced at 600 °C in H_2 is 1.74 mol_{CO} g_{Au}^{-1} h^{-1} and 6 times higher than the Au catalyst. After the oxidation treatment of the Au−Ni catalyst at 400 °C, the specific reaction rate is 1.49 mol_{CO} g_{Au}^{-1} h^{-1}, which is still quite high. However, the subsequent oxidation at 600 °C decreases the rate down to 0.85 mol_{CO} g_{Au}^{-1} h^{-1}. The active Au−Ni/SiO_2 catalysts exhibit much higher activity than the Au-organic-SiO_2 catalyst (0.48 mol_{CO} g_{Au}^{-1} h^{-1}) reported by Corma and Budroni and Au/SiO_2 catalysts prepared by chemical vapor deposition (0.17 mol_{CO} g_{Au}^{-1} h^{-1})[40,41] and are comparable to the well-known active Au/TiO_2 catalysts (2.32 mol_{CO} g_{Au}^{-1} h^{-1}).[42]

3.2. TEM and XRD Structural Characterization. TEM investigations show that metal nanoparticles in the as-prepared Au/SiO_2 and Au−Ni/SiO_2 samples exhibit narrow size distribution, having average sizes of 2.1 and 2.6 nm, respectively (Figure 4). The average size of Au NPs for the Au/SiO_2 catalyst increases to 4.5 nm after reduction at 600 °C. For the Au−Ni/SiO_2 catalysts, the particle sizes change to 3.5 nm after the same treatment. The comparative studies indicate that the presence of Ni components in the Au−Ni samples effectively prevents sintering of the nanoparticles at elevated temperatures.

XRD pattern (Figure 5A) of the Au−Ni/SiO_2 sample oxidized at 600 °C shows the same Au(111) peak position as that of the Au/SiO_2 sample, which is located at 38.2. Neither Ni nor NiO phases were detected in the Au−Ni/SiO_2 catalysts, suggesting that Ni may exist as highly dispersed species. With the subsequent reduction at 600 °C, the Au(111) peak shifts to a higher angle at 38.6, but the peak shift is not obvious when reduced at low temperatures. It is reported that the Au(111) diffraction peak for Au_1Ni_1 alloy shifts to 40.7.[43] Thus, the observed small shift in our case suggests that only a small part of the surface Ni species (about 12.5% of total Ni atoms as calculated by the Vegard's law) has been alloyed with Au NPs

dx.doi.org/10.1021/cs400197t | ACS Catal. 2013, 3, 1810−1818

Table 1. Catalytic Activity for CO Oxidation over the Au/SiO_2 and $Au-Ni/SiO_2$ Catalysts Treated under Different Conditions[a]

samples	treatments	loading of Au (%)	TM/Au (atom ratio)	specific rates (mol_{CO} g_{Au}^{-1} h^{-1})	E_{app}(LT) (kJ/mol)	E_{app}(HT) (kJ/mol)
Au/SiO_2	H_2@600 °C	4.4	0/1	0.26		75
$Au-Ni/SiO_2$	H_2@600 °C	4.5	1.1/1	1.74	3.0	29
$Au-Ni/SiO_2$	H_2@600 °C/O_2@400 °C	4.5	1.1/1	1.49	4.1	30
$Au-Ni/SiO_2$	H_2@600 °C/O_2@600 °C	4.5	1.1/1	0.85		68
$Au-Co/SiO_2$	H_2@600 °C	4.5	1.2/1	1.91	3.8	38
$Au-Fe/SiO_2$	H_2@600 °C	4.9	0.9/1	0.96	4.9	34

[a]The actual loadings of Au and transition metals were determined by ICP. For specific reaction rate measurements, 6 mg of catalyst was diluted with SiC powder, and the reactions were carried out under the kinetic-limiting region by controlling GHSV.

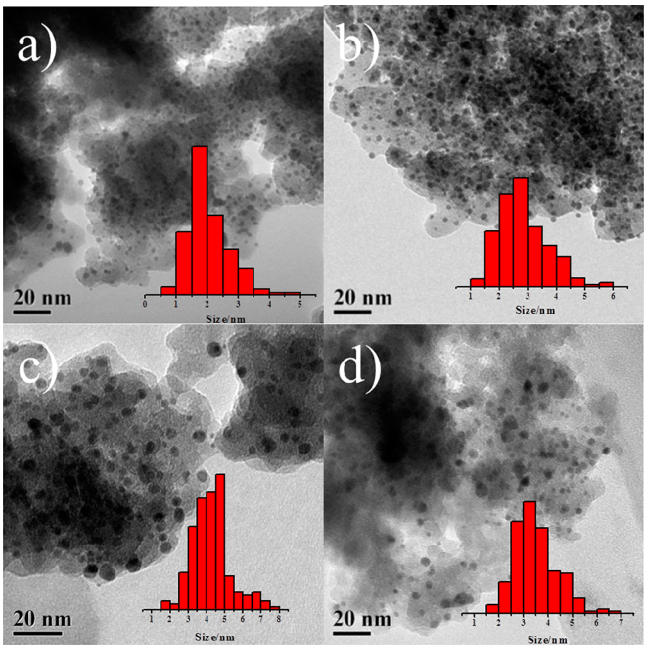

Figure 4. TEM images and derived particle size distribution from as-prepared Au/SiO_2 sample (a), as-prepared $Au-Ni/SiO_2$ sample (b), the Au/SiO_2 sample reduced at 600 °C (c), and the $Au-Ni/SiO_2$ sample reduced at 600 °C (d).

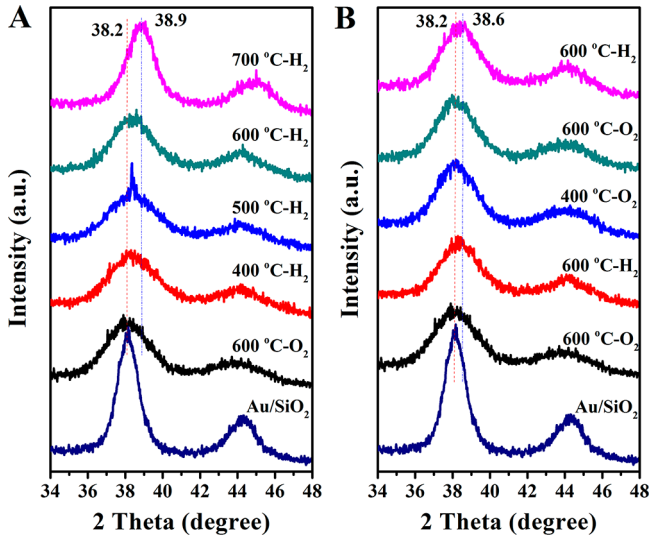

Figure 5. XRD patterns acquired from the $Au-Ni/SiO_2$ sample reduced at different temperatures (A) and the $Au-Ni/SiO_2$ sample subjected to cycled redox treatments (B). The sequence is from the bottom to the top in the figures. For comparison, a pattern from the Au/SiO_2 sample reduced at 600 °C was also included.

upon reduction at 600 °C. The peak position further shifts to 38.9 in the $Au-Ni/SiO_2$ sample when reduced at 700 °C, and thus more Ni species can diffuse inside of Au NPs under the higher temperature reduction condition.

Starting from the $Au-Ni/SiO_2$ sample reduced at 600 °C, oxidation at 400 and 600 °C causes the shift of the Au(111) diffraction peak back to 38.2 (Figure 5B). After the second reduction treatment at 600 °C over the oxidized sample, the peak can shift to 38.6 again. The reversible structural changes in the Au–Ni NPs with response to the redox treatments clearly show that the surface Ni atoms can diffuse inside of Au NPs when annealing in a H_2 atmosphere at elevated temperatures, while the alloyed Ni atoms may segregate to the particle surfaces driven by the oxidation treatments. The similar reversible inward and outward diffusion of transition metal atoms at Pt surfaces also occurs with the cycled redox treatments.[44−46]

The average size of Au NPs for $Au-Ni/SiO_2$ samples reduced at 600 °C was calculated to be 4.0 nm using Scherrer's equation, which is much smaller than that (5.7 nm) of the Au/SiO_2 catalyst with the same treatments. The XRD result is consistent with the above TEM data, confirming that the sintering of Au NPs in the $Au-Ni/SiO_2$ samples has been effectively suppressed by the surface Ni components.

3.3. Chemical State Analysis from XPS and XAS. Ex situ XPS measurements were performed over $Au-Ni/SiO_2$ catalysts, which were treated under different conditions and then exposed to the air at RT before XPS analysis. In the investigated $Au-Ni/SiO_2$ catalysts, the Au components always keep metallic with Au $4f_{7/2}$ located at 83.9 eV, irrespective of the various treatments (Figures 6A and 7A). However, the XPS Ni 2p spectrum changes largely during these processes (Figures 6B and 7B). For the as-prepared $Au-Ni/SiO_2$ sample calcined in the air at 600 °C, the XPS Ni $2p_{3/2}$ spectrum consists of two components that peak at 856.9 and 862.1 eV, which are ascribed to the main peak of Ni oxide and the corresponding satellite peak, respectively. It is known that the Ni $2p_{3/2}$ main peak from a bulk NiO surface presents a main line at 854.5 eV and a shoulder shifted around 1.7 eV toward higher binding energy from the main line. The main line comes from Ni atoms octahedrally coordinated in the bulk, and the shoulder has been attributed to pyramidally coordinated Ni atoms at the NiO surface and the nonlocal screening effect.[47,48] The shape and position of the Ni $2p_{3/2}$ main peak can change in the case of supported NiO nanostructures. Due to the high percentage of surface Ni component, the shoulder signal may become dominant in the main peak such that the Ni $2p_{3/2}$ main peak shifts to a higher binding energy position.[49,50] Accordingly, we

dx.doi.org/10.1021/cs400197t | ACS Catal. 2013, 3, 1810−1818

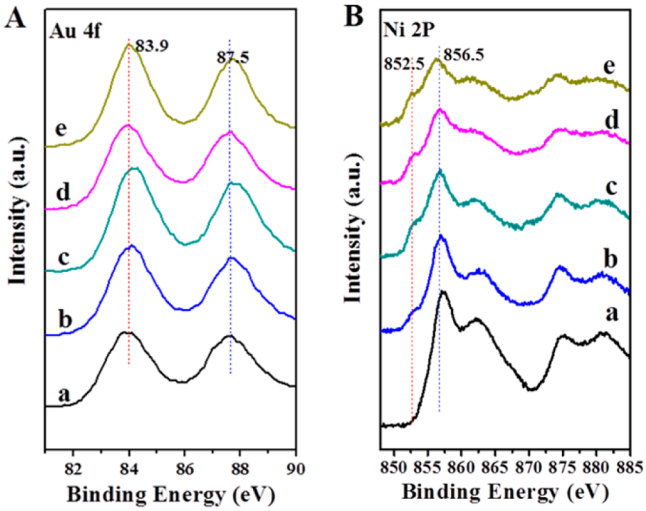

Figure 6. XPS Au 4f (A) and Ni 2p (B) spectra from the Au−Ni/SiO_2 catalyst subjected to sequential treatments: (a) oxidation at 600 °C, (b) reduction at 400 °C, (c) reduction at 500 °C, (d) reduction at 600 °C, (e) reduction at 700 °C.

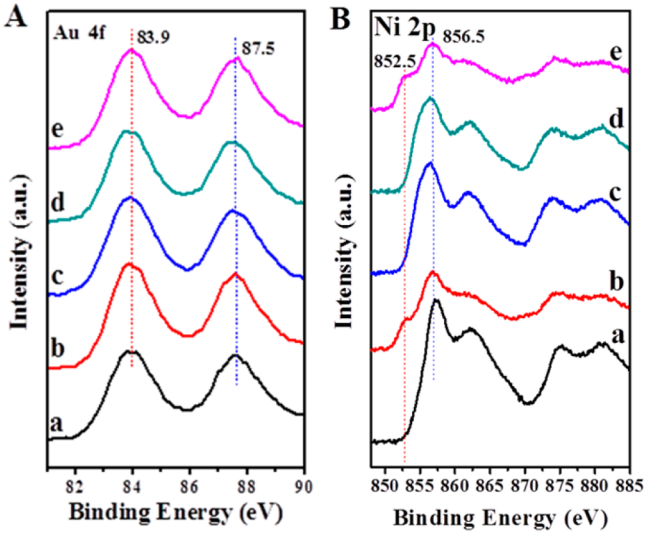

Figure 7. XPS Au4f (A) and Ni2p (B) spectra from the Au−Ni/SiO_2 catalyst subjected to sequential treatments: (a) oxidation at 600 °C, (b) reduction at 600 °C, (c) reoxidation at 400 °C, (d) reoxidation at 600 °C, (e) second reduction at 600 °C.

suggest that the main peak located at 856.9 eV should be attributed to the highly dispersed NiO aggregates supported on Au NPs, which is similar to the report from Naumkin and co-workers.[51]

Reduction of the Au−Ni/SiO_2 catalysts changes the line shape of Ni 2p spectra (Figures 6B and 7B). Besides the components at 856.5 and 861.5 eV, a new feature appears at 852.5 eV, which comes from metallic Ni species. This result indicates that both Ni and NiO species are present in the reduced samples. Our previous works on Pt−Ni/carbon black catalysts have shown that Ni species at the surfaces of support and Pt NPs are prone to getting oxidized when exposed to air, while the Ni atoms at the subsurface regions of Pt NPs remain metallic due to the protection by surface noble metal overlayers.[32,44,52] Therefore, we suggest that the observed NiO in the Au−Ni catalysts should be from the Ni species on the surfaces of SiO_2 support and Au NPs. The metallic Ni species are due to alloyed Ni atoms inside of Au NPs, which are free from oxidation in the air. With the increase in the reduction temperature, the ratio of the Ni component to the NiO component in the Ni $2p_{3/2}$ spectra keeps on increasing (Figure 6B and Table 2), indicating that more Ni atoms can diffuse inside of Au NPs at higher reduction temperatures. The ratio of Ni to Ni^{2+} is 0.26 even after heating in H_2 at 700 °C, and thus, most of the Ni species are still outside of NPs after the reduction treatments. At the same time, reduction of the Au−Ni/SiO_2 catalysts weakens the Ni 2p spectrum intensity. The area ratio of Ni $2p_{3/2}$ to Au $4f_{7/2}$ decreases from 4.7 for the oxidized Au−Ni/SiO_2 sample to 1.6 for the sample reduced at 700 °C (Table 2). Again, the reduction treatment induces inward diffusion of surface Ni species into Au NPs, which attenuates the Ni 2p intensity.

The peak at 852.5 eV disappears after the subsequent oxidation at 400 and 600 °C (Figure 7B). The oxidation treatments also increase the area ratio between Ni $2p_{3/2}$ and Au $4f_{7/2}$ (Table 2). Therefore, the oxidation treatments drive the surface segregation of alloyed Ni atoms from the core regions of Au NPs. The second reduction at 600 °C causes reappearance of the metallic Ni XPS component at 852.5 eV and a lower area ratio of Ni $2p_{3/2}$ to Au $4f_{7/2}$, which is due to the reduction-induced inward diffusion of surface Ni atoms.

Figure 8 displays the k^2-weighted Fourier transformed (FT) EXAFS spectra recorded from Au−Ni/SiO_2 catalysts treated differently. The FT EXAFS oscillations of Ni foil show that there is one peak corresponding to the first coordination shell of metallic Ni with a Ni−Ni distance at 2.2 Å. In the spectrum from a standard NiO sample, a coordination shell of Ni−Ni

Table 2. XPS Analysis of Au/SiO_2 and Au−Ni/SiO_2 Catalysts Treated under Different Conditions[a]

samples	treatments	Au $4f_{7/2}$ (ev)	Ni $2p_{3/2}$ main peak (eV)	Ni $2p_{3/2}$ shoulder (eV)	Ni^0/Ni^{2+} (area ratio)	Ni $2p_{3/2}$/Au $4f_{7/2}$ (area ratio)
Au/SiO_2	H_2@600 °C	83.8				
Au−Ni/SiO_2	O_2@600 °C	83.9	856.9			4.7
Au−Ni/SiO_2	H_2@400 °C	84.0	856.5	852.5	0.10	2.2
Au−Ni/SiO_2	H_2@500 °C	84.0	856.5	852.5	0.20	1.9
Au−Ni/SiO_2	H_2@600 °C	84.0	856.5	852.5	0.24	1.8
Au−Ni/SiO_2	H_2@700 °C	84.0	856.3	852.4	0.26	1.6
Au−Ni/SiO_2	H_2@600 °C/O_2@400 °C	83.9	856.5			3.1
Au−Ni/SiO_2	H_2@600 °C/O_2@600 °C	83.9	856.5			2.9
Au−Ni/SiO_2	H_2@600 °C again	83.9	856.5	852.4	0.32	1.7

[a] Ni^{2+}: Ni oxide. Ni^0: metallic Ni.

dx.doi.org/10.1021/cs400197t | ACS Catal. 2013, 3, 1810−1818

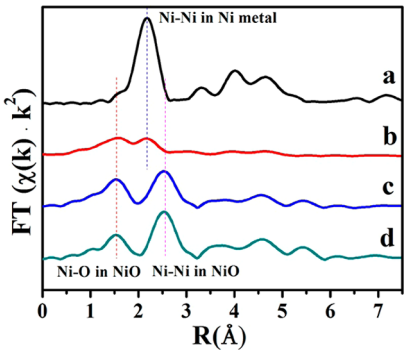

Figure 8. The magnitudes of the k^2-weighted Fourier transformed EXAFS spectra recorded from Ni foil (a), the Au−Ni/SiO_2 catalyst reduced at 600 °C (b), the reduced Au−Ni/SiO_2 catalyst subjected to further oxidation treatment at 400 °C (c), and a NiO standard sample (d).

with a distance of 2.5 Å and a coordination shell Ni−O with a distance of 1.5 Å are present. The FT EXAFS spectrum of the Au−Ni/SiO_2 sample reduced at 600 °C consists of contributions from the Ni−Ni coordination information of metallic Ni and the Ni−O coordination information of NiO. Thus, a substantial amount of Ni species are still outside of Au NPs in this sample, which get oxidized in the air. With the oxidation at 400 °C, the FT EXAFS spectrum is very similar to that of NiO, which suggests that all Ni atoms have been oxidized by the oxidation treatment, consistent with the XPS and XRD results.

4. DISCUSSIONS

4.1. Structure Changes of Au−Ni Catalysts with Redox Treatments. On the basis of the structural characterization results, we suggest that a surface architecture consisting of a Au-rich core and a Ni(NiO)-rich shell is present in the as-prepared Au−Ni samples prepared by the two-step synthetic method. Silica supported Au NPs were first synthesized, and the formed Au NPs have been negatively charged.[53−55] The added Ni^{2+} ions can be preferentially absorbed onto the Au surfaces via electrostatic attraction. Furthermore, the negatively charged Au NPs also facilitate the reduction of Ni^{2+} ions, as reported by some groups.[54,56] The strong interaction between Au NPs and Ni cations helps to produce Ni-decorated Au NPs, which transform to NiO-decorated Au NPs when exposed to the air or heated in O_2.

The treatment in H_2 and at 600 °C can reduce the surface Ni oxide to metallic Ni and, further, drive small part of surface Ni atoms to diffuse into the Au cores, as confirmed by our XPS, XRD, and EXAFS. The surface energy of Au is much smaller (1.33 j·m^{-2}) than that of Ni (2.08 j m^{-2}). Therefore, surface Ni atoms tend to diffuse into the Au subsurface regions while Au atoms segregate to the topmost surface when annealing in a vacuum or reductive atmospheres.[57] For example, at a Ni/Au(111) surface extensive Au segregation to the top surface has been observed when annealing the surface at 510 K in an ultrahigh vacuum, and all surface Ni atoms diffuse into the bulk after further annealing up to 630 K.[58] However, the large immiscibility between Au and Ni at low temperature ranges makes the AuNi alloy formation difficult below 600 °C.[43,59] This is different from Au−Ag and Au−Cu systems, in which the alloy structures can form around 300 °C.[24,28,60]

With the subsequent oxidation treatment at 400 °C, the Ni atoms alloyed with Au NPs segregate to the particle surfaces and form highly dispersed NiO nanopatches. Transition metals such as Fe, Co, Ni, and Cu have a stronger oxygen affinity than Au. It is expected that the transition metal tends to segregate to surfaces and get oxidized under oxidative conditions.[27,28,43,61] With the oxidation treatment at a much higher temperature, e.g. above 600 °C, the surface NiO nanopatches may form aggregates, lowering the NiO−Au boundary density. The structure change of Au−Ni NPs with the redox treatments can be illustrated by the schematics shown in Figure 9.

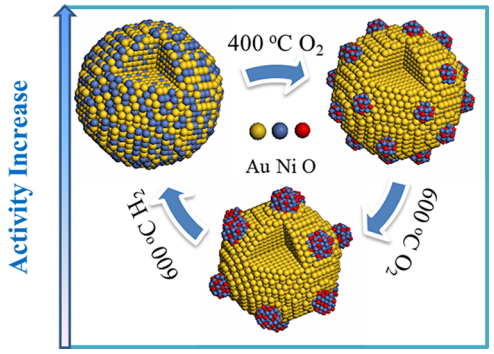

Figure 9. Schematics showing the variation of the surface architecture of Au−Ni nanoparticles with the redox treatments. The change in activity was also illustrated.

It should be pointed out that the APTES surfactant at the silica surface may affect the structural change with the treatment. If the as-prepared Au−Ni/SiO_2 sample was annealed in Ar at 600 °C without initial calcination, the catalyst presents quite low activity to CO oxidaiton, even worse than the Au/SiO_2 catalyst (Figure 10A). XPS measurement of the Ar-treated sample shows that there is a substantial amount of carbon at the surface, and moreover, the Ni 2p spectrum is dominated by Ni^0 state (Figure 10B). We infer that the metal catalyst may be encapsulated by carbon overlayers formed from the decomposition of APTES surfacant during the Ar treatment process, such that Ni remains metallic in the air and the surface activity gets deteriorated. The subsequent oxidation at 400 °C enhanced the reactivity significantly, and the CO conversion reached 90% at RT (Figure 10A). Now, the main peak of Ni $2p_{3/2}$ shifts to 856.5 eV, corresponding to the NiO structure, and the peak area increases largely (Figure 10B). The oxidation process etched the surface carbon and produced the architecutre of NiO-decorated Au NPs. Therefore, the as-prepared catalysts need to be treated in O_2 or H_2 above 400 °C to avoid the surfactant effect.

4.2. Active Structure of Au−Ni Catalysts for CO Oxidation. According to the above studies in the structure−activity relationship, the enhanced catalytic performance of the Au−Ni catalysts can be attributed to the synergistic effect between Au and NiO components. The highly active Au−Ni/SiO_2 catalysts should have the surface architecture containing Au NPs decorated by highly dispersed NiO nanopatches, i.e. NiO-on-Au surface structure. For the Au−Ni NPs reduced at 600 °C, a small part of Ni atoms diffuse inside of NPs while the left remain at the particle surfaces, probably forming a Ni-rich surface alloy structure. When exposed to the air or oxidative reaction gases, the surface Ni atoms get oxidized and form surface NiO nanostructures. Subsequent oxidation of the

dx.doi.org/10.1021/cs400197t | ACS Catal. 2013, 3, 1810−1818

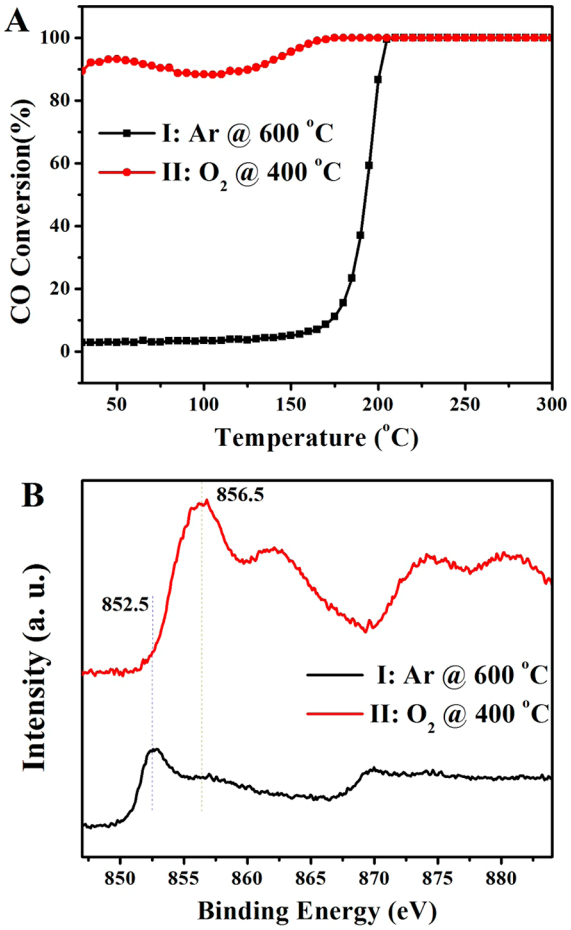

Figure 10. (A) CO conversion light-off curve over the Au−Ni/SiO_2 catalyst treated in Ar at 600 °C and O_2 at 400 °C, successively. (B) XPS Ni2p spectra from the two catalysts.

sample at a low temperature, e.g. 400 °C, drives the surface segregation of the alloyed Ni atoms and produces highly dispersed NiO nanopatches. Thus, it is expected that the two samples present the best CO oxidation activity among all catalysts (Figure 3).

Pure Au/SiO_2 catalyst exhibits negative apparent activation energy in the low temperature region and high apparent activation energy in the high temperature region (75 kJ/mol). For the Au−Ni/SiO_2 catalyst reduced at 600 °C, the apparent activation energy in the low temperature range is 3.0 kJ/mol and that for the high temperature region is 29 kJ/mol. Those for the Au−Ni/SiO_2 catalyst with one more step of oxidation at 400 °C are quite similar (Table 1). In the low temperature region, the CO oxidation over Au−Ni nanocatalysts may proceed via multiple mechanisms. CO absorbed on Au NPs can react with weakly absorbed O_2 species or surface hydroxyl groups on the Au surface, which is similar to the reaction over pure Au catalysts and presents negative activation energy.[39] Moreover, the interface between Au and NiO contributes to the activity through reaction of CO molecules absorbed on Au NPs with adjacent dissociated oxygen atoms at the oxide edges.[29] Accordingly, it may be expected that quite low apparent activation energy toward CO oxidation has been observed in the low temperature region. The low activation energy values ranging from 2.1 to 13.4 kJ/mol have also been measured for the CO oxidation over Au/TiO_2 and Au/Fe_2O_3 catalysts.[62−65] In the high temperature region, the reaction mainly proceeds via the bifunctional reaction mechanism, and O_2 dissociation is the limiting step. In our NiO-on-Au catalysts, the formed NiO−Au boundaries provide the active sites for O_2 activation, and the presence of NiO nanopatches on Au surfaces can significantly enhance the intrinsic activity toward CO oxidation. Recently, Zhou et al. reported that the inert Au film decorated with ceria nanoparticles shows an enhanced activity of about 3 orders of magnitude. The reaction mainly occurs at the interface between ceria nanoparticles and Au films with an apparent activation energy of 49 ± 9 kJ/mol.[66] The addition of Fe_2O_3 nanoclusters can transform the inert Au(111) single crystal into an active catalyst for CO oxidation, and the apparent activation energy was measured just at 20 ± 4 kJ/mol.[67]

The oxidation treatment at 600 °C deteriorates the surface reactivity, and the apparent activation energy is 68 kJ/mol in the high temperature region, which is close to that of the Au/SiO_2 catalyst. Probably, the high temperature oxidation treatment causes aggregation of surface NiO species and decreases the density of NiO/Au boundary.

The critical role of surface NiO nanopatches in the Au-catalyzed CO oxidation can be further confirmed by a leaching experiment. The active Au−Ni/SiO_2 catalyst, which has been treated in H_2 at 600 °C, was washed in a nitric acid solution. The leaching process has removed 85% of the Ni species, and the remaining 15% may remain inside of Au NPs or strongly bond with silica surfaces. After the same activation of the leached sample in H_2 at 600 °C, the catalyst presents much low activity for the CO oxidation at low temperature (Figure 11).

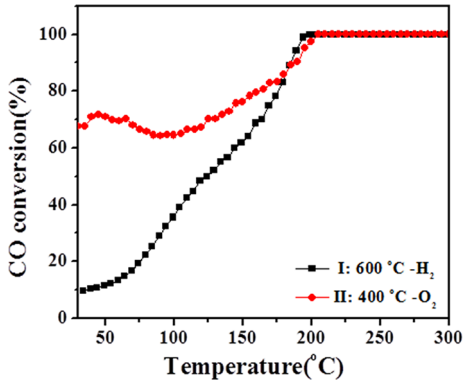

Figure 11. CO conversion light-off curves over a leached Au−Ni/SiO_2 catalyst treated in H_2 at 600 °C and in O_2 at 400 °C, successively.

The specific reaction rate is only 0.07 $mol_{CO}\ g_{Au}^{-1}\ h^{-1}$ at 30 °C, even lower than that of Au/SiO_2. Unlike the pure Au/SiO_2 catalyst, the leached sample shows an increasing activity with temperature, indicating that residual Ni atoms inside of nanoparticles start to segregate to the surface at increasing reaction temperatures and contribute to the reactivity. Oxidation of this sample at 400 °C has increased the specific reaction rate to 0.52 $mol_{CO}\ g_{Au}^{-1}\ h^{-1}$, and the activity in the whole reaction temperature range becomes higher. Nevertheless, it is still much less active than the catalyst before leaching. A small valley also appears in the activity curve, indicating that the reaction also occurs via the low-temperature and high-temperature mechanisms. The apparent activation energy for the oxidized sample in the high temperature region is about 26 kJ/mol, close to that of the most active Au−Ni/SiO_2 catalysts. The result suggests that active sites and the reaction pathway over the leached sample are the same as that

dx.doi.org/10.1021/cs400197t | ACS Catal. 2013, 3, 1810−1818

of the active Au−Ni/SiO_2 catalysts. The leaching removes surface NiO species, lowering the surface activity, while oxidation of the leached sample produces surface NiO species, enhancing the activity again.

Considering that the boundary between NiO and Au plays a critical role in the reaction, we expect that there should be an optimum coverage of surface Ni (NiO) species on the Au surface. The volcano-type dependence of the CO oxidation activity on the Ni/Au ratio (Figure 1) illustrates this point very well. At an intermediate coverage of NiO, the NiO/Au boundary density becomes maximized such that the highest activity has been observed.

On the basis of the results, we conclude that the NiO-on-Au surface structure is highly active for the CO oxidation, and the active sites should be located at the perimeters of NiO nanopatches. The ensembles at the NiO-Au boundaries provide dual sites for O_2 activation and CO adsorption, similar to TMO-on-Pt inverse systems.[29,68]

4.3. TMO-on-Au Architecture for CO Oxidation. All the results clearly illustrate the critical role of surface NiO structures in the enhanced reaction performance of Au−Ni catalysts. Particularly, the boundaries between Au NPs and NiO nanopatches act as the active sites for the CO oxidation, and a maximum in the surface activity can be achieved by constructing a high density of oxide/Au boundaries. In our previous works, we have shown that the TMO-on-Pt inverse catalysts are highly active in CO oxidation reactions, and the TMO/Pt interfaces have been identified as the active sites. The proposed interface confinement effect has been successfully applied in FeO-on-Pt, CoO-on-Pt, and NiO-on-Pt catalysts.[29,31−34] To reveal whether the TMO-on-Au active structure for the CO oxidation can be extended to other transition metal oxides, Au−Co/SiO_2 and Au−Ni/SiO_2 catalysts were prepared by the same two-step synthetic method to have CoO_x-on-Au and NiO_x-on-Au structures. Both catalysts were treated in H_2 at 600 °C and then subjected to the same CO oxidation test. The specific reaction rates at 30 °C for the Au−Co/SiO_2 and Au−Fe/SiO_2 catalysts are 1.91 $mol_{CO}\ g_{Au}^{-1}\ h^{-1}$ and 0.96 $mol_{CO}\ g_{Au}^{-1}\ h^{-1}$, respectively (Table 1), which are much higher than that of the Au/SiO_2 catalyst. In the low temperature region, the apparent activation energy values for the Au−Co/SiO_2 and Au−Ni/SiO_2 catalysts are 3.8 and 4.9 kJ/mol, and those in the high temperature range are 38 and 34 kJ/mol (Table 1). They are quite similar to the active Au−Ni/SiO_2 catalysts, indicating that CO oxidation over these catalysts proceeds by similar reaction pathways. The results show the strong promotional effect of surface Fe oxide and Co oxide nanostructures on the Au-catalyzed CO oxidation reaction.

Recent works on Au/CeO_2 and Fe_2O_3/Au model catalysts illustrate the critical role of the oxide/Au interface in the CO oxidation.[66,67,69] In Au/CeO_2 multilayer nanotowers, CO oxidation rates were scaled with the total length of Au/CeO_2 interface.[69] Excellent catalytic performance over supported Au−Cu, Au−Ni, and Au−Fe nanocatalysts has been observed,[27,43,70−72] in which the oxide/Au ensembles have been identified as the active structure as well. On the basis of the results, it can be inferred that Au catalysis can be strongly promoted by the synergetic effect between Au and TMO, and the TMO-on-Au inverse architecture may be active in many Au-catalyzed reactions. Previous works have demonstrated that high activity can be realized using Au clusters with lower amount of Au.[14,73,74] In the present TMO-on-Au catalysts, the interfaces formed between TMO overlayers and Au surfaces are controlling the reactions, and most Au atoms inside the NPs are useless. The minimization of Au amount can be achieved using smaller Au NPs or Au-shell nanostructures as support for TMO nanostructures, as we did in the FeO-on-Cu@Pt catalysts.[75] Furthermore, the TMO-on-Au catalysts can be applied in other reactions, such as water-gas shift and alcohol oxidation.

5. CONCLUSION

The synergistic effect between Au and Ni components makes supported Au−Ni nanocatalysts highly active toward CO oxidation and, moreover, prevents sintering of Au NPs at high temperatures. Structural studies in the supported Au−Ni nanocatalysts confirm that a small part of surface Ni atoms can diffuse into Au cores upon reduction at 600 °C, while the alloyed Ni atoms segregate to the top surface when oxidized at a similar temperature. Both inward and outward diffusion of Ni atoms at Au NP surfaces are reversible with response to the cycled reduction and oxidation treatments. CO oxidation results show that the active Au−Ni surface architecture consists of Au NPs decorated with highly dispersed NiO nanopatches. The optimum activity has been obtained by constructing high density NiO/Au boundary sites in the NiO-on-Au inverse catalysts. Both surface Co oxide and Fe oxide are found to promote the Au-catalyzed CO oxidation reaction as well, suggesting the highly active TMO-on-Au architecture.

AUTHOR INFORMATION

Corresponding Author

*Fax: (+86)-411-84694447. E-mail: qfu@dicp.ac.cn.

Notes

The authors declare no competing financial interest.

ACKNOWLEDGMENTS

This work was financially supported by the National Natural Science Foundation of China (No. 21222305, No. 11079005, and No. 20923001) and Ministry of Science and Technology of China (No. 2013CB834603, No. 2011CBA00503, and No. 2013CB933100).

REFERENCES

(1) Haruta, M.; Yamada, N.; Kobayashi, T.; Iijima, S. *J. Catal.* **1989**, *115*, 301.
(2) Hughes, M. D.; Xu, Y. J.; Jenkins, P.; McMorn, P.; Landon, P.; Enache, D. I.; Carley, A. F.; Attard, G. A.; Hutchings, G. J.; King, F.; Stitt, E. H.; Johnston, P.; Griffin, K.; Kiely, C. J. *Nature* **2005**, *437*, 1132.
(3) Abad, A.; Concepcion, P.; Corma, A.; Garcia, H. *Angew. Chem., Int. Ed.* **2005**, *44*, 4066.
(4) Corma, A.; Serna, P. *Science* **2006**, *313*, 332.
(5) Bond, G. C.; Thompson, D. T. *Catal. Rev.* **1999**, *41*, 319.
(6) Haruta, M.; Date, M. *Appl. Catal., A* **2001**, *222*, 427.
(7) Kung, M. C.; Davis, R. J.; Kung, H. H. *J. Phys. Chem. C* **2007**, *111*, 11767.
(8) Schubert, M. M.; Hackenberg, S.; van Veen, A. C.; Muhler, M.; Plzak, V.; Behm, R. J. *J. Catal.* **2001**, *197*, 113.
(9) Fujitani, T.; Nakamura, I. *Angew. Chem., Int. Ed.* **2011**, *50*, 10144.
(10) Widmann, D.; Behm, R. J. *Angew. Chem., Int. Ed.* **2011**, *50*, 10241.
(11) Kim, H. Y.; Lee, H. M.; Henkelman, G. *J. Am. Chem. Soc.* **2012**, *134*, 1560.
(12) Liu, Z.-P.; Gong, X.-Q.; Kohanoff, J.; Sanchez, C.; Hu, P. *Phys. Rev. Lett.* **2003**, *91*, 266102.

(13) Green, I. X.; Tang, W.; Neurock, M.; Yates, J. T. *Science* **2011**, *333*, 736.
(14) Hutchings, G.; Hall, M.; Carley, A.; Landon, P.; Solsona, B.; Kiely, C.; Herzing, A.; Makkee, M.; Moulijn, J.; Overweg, A. *J. Catal.* **2006**, *242*, 71.
(15) Liu, X.; Liu, M.-H.; Luo, Y.-C.; Mou, C.-Y.; Lin, S. D.; Cheng, H.; Chen, J.-M.; Lee, J.-F.; Lin, T.-S. *J. Am. Chem. Soc.* **2012**, *134*, 10251.
(16) Zhang, J.; Sasaki, K.; Sutter, E.; Adzic, R. R. *Science* **2007**, *315*, 220.
(17) Yamauchi, Y.; Tonegawa, A.; Komatsu, M.; Wang, H.; Wang, L.; Nemoto, Y.; Suzuki, N.; Kuroda, K. *J. Am. Chem. Soc.* **2012**, *134*, 5100.
(18) Zhang, S.; Shao, Y.; Liao, H.-g.; Liu, J.; Aksay, I. A.; Yin, G.; Lin, Y. *Chem. Mater.* **2011**, *23*, 1079.
(19) Enache, D. I.; Edwards, J. K.; Landon, P.; Solsona-Espriu, B.; Carley, A. F.; Herzing, A. A.; Watanabe, M.; Kiely, C. J.; Knight, D. W.; Hutchings, G. J. *Science* **2006**, *311*, 362.
(20) Chen, M. S.; Kumar, D.; Yi, C. W.; Goodman, D. W. *Science* **2005**, *310*, 291.
(21) Zhou, W.; Lee, J. Y. *Electrochem. Commun.* **2007**, *9*, 1725.
(22) Xu, J.; White, T.; Li, P.; He, C. H.; Yu, J. G.; Yuan, W. K.; Han, Y. F. *J. Am. Chem. Soc.* **2010**, *132*, 10398.
(23) Wang, A. Q.; Liu, J. H.; Lin, S. D.; Lin, T. S.; Mou, C. Y. *J. Catal.* **2005**, *233*, 186.
(24) Sandoval, A.; Aguilar, A.; Louis, C.; Traverse, A.; Zanella, R. *J. Catal.* **2011**, *281*, 40.
(25) Rodriguez, J. A.; Ma, S.; Liu, P.; Hrbek, J.; Evans, J.; Perez, M. *Science* **2007**, *318*, 1757.
(26) Rameshan, C.; Stadlmayr, W.; Penner, S.; Lorenz, H.; Memmel, N.; Hävecker, M.; Blume, R.; Teschner, D.; Rocha, T.; Zemlyanov, D.; Knop-Gericke, A.; Schlögl, R.; Klötzer, B. *Angew. Chem., Int. Ed.* **2012**, *51*, 3002.
(27) Li, X.; Fang, S. S. S.; Teo, J.; Foo, Y. L.; Borgna, A.; Lin, M.; Zhong, Z. *ACS Catal.* **2012**, *2*, 360.
(28) Liu, X.; Wang, A.; Li, L.; Zhang, T.; Mou, C.-Y.; Lee, J.-F. *J. Catal.* **2011**, *278*, 288.
(29) Fu, Q.; Yang, F.; Bao, X. *Acc. Chem. Res.* **2013**, DOI: 10.1021/ar300249b.
(30) Surnev, S.; Fortunelli, A.; Netzer, F. P. *Chem. Rev.* **2013**, *113*, 4314.
(31) Fu, Q.; Li, W.-X.; Yao, Y.; Liu, H.; Su, H.-Y.; Ma, D.; Gu, X.-K.; Chen, L.; Wang, Z.; Zhang, H.; Wang, B.; Bao, X. *Science* **2010**, *328*, 1141.
(32) Mu, R.; Fu, Q.; Xu, H.; Zhang, H.; Huang, Y.; Jiang, Z.; Zhang, S.; Tan, D.; Bao, X. *J. Am. Chem. Soc.* **2011**, *133*, 1978.
(33) Xu, H.; Fu, Q.; Yao, Y.; Bao, X. *Energy Environ. Sci.* **2012**, *5*, 6313.
(34) Xu, H.; Fu, Q.; Guo, X.; Bao, X. *ChemCatChem* **2012**, *4*, 1645.
(35) Khan, N. A.; Matranga, C. *Surf. Sci.* **2008**, *602*, 932.
(36) Bao, F.; Li, J.-F.; Ren, B.; Yao, J.-L.; Gu, R.-A.; Tian, Z.-Q. *J. Phys. Chem. C* **2008**, *112*, 345.
(37) Liu, X.; Wang, A.; Wang, X.; Mou, C.-Y.; Zhang, T. *Chem. Commun.* **2008**, 3187.
(38) Qian, K.; Huang, W.; Fang, J.; Lv, S.; He, B.; Jiang, Z.; Wei, S. *J. Catal.* **2008**, *255*, 269.
(39) Daté, M.; Okumura, M.; Tsubota, S.; Haruta, M. *Angew. Chem., Int. Ed.* **2004**, *43*, 2129.
(40) Budroni, G.; Corma, A. *Angew. Chem., Int. Ed.* **2006**, *45*, 3328.
(41) Okumura, M.; Nakamura, S.; Tsubota, S.; Nakamura, T.; Azuma, M.; Haruta, M. *Catal. Lett.* **1998**, *51*, 53.
(42) Bamwenda, G. R.; Tsubota, S.; Nakamura, T.; Haruta, M. *Catal. Lett.* **1997**, *44*, 83.
(43) Zhou, S.; Yin, H.; Schwartz, V.; Wu, Z.; Mullins, D.; Eichhorn, B.; Overbury, S. H.; Dai, S. *ChemPhysChem* **2008**, *9*, 2475.
(44) Mu, R.; Fu, Q.; Liu, H.; Tan, D.; Zhai, R.; Bao, X. *Appl. Surf. Sci.* **2009**, *255*, 7296.
(45) Ma, T.; Fu, Q.; Su, H.-Y.; Liu, H.-Y.; Cui, Y.; Wang, Z.; Mu, R.-T.; Li, W.-X.; Bao, X.-H. *ChemPhysChem* **2009**, *10*, 1013.
(46) Ma, T.; Fu, Q.; Cui, Y.; Zhang, Z.; Wang, Z.; Tan, D.; Bao, X. *Chin. J. Catal.* **2010**, *31*, 24.
(47) Mossanek, R. J. O.; Preda, I.; Abbate, M.; Rubio-Zuazo, J.; Castro, G. R.; Vollmer, A.; Gutiérrez, A.; Soriano, L. *Chem. Phys. Lett.* **2011**, *501*, 437.
(48) Grosvenor, A. P.; Biesinger, M. C.; Smart, R. S.; McIntyre, N. S. *Surf. Sci.* **2006**, *600*, 1771.
(49) Preda, I.; Gutierrez, A.; Abbate, M.; Yubero, F.; Mendez, J.; Alvarez, L.; Soriano, L. *Phys. Rev. B* **2008**, *77*, 07541.
(50) Preda, I.; Mossanek, R. J. O.; Abbate, M.; Alvarez, L.; Mendez, J.; Gutierrez, A.; Soriano, L. *Surf. Sci.* **2012**, *606*, 1426.
(51) Naumkin, A. V.; Vasil'kov, A. Y.; Volkov, I. O.; Smirnov, V. V.; Nikolaev, S. A. *Inorg. Mater.* **2007**, *43*, 381.
(52) Mu, R.; Guo, X.; Fu, Q.; Bao, X. *J. Phys. Chem. C* **2011**, *115*, 20590.
(53) Shipway, A. N.; Lahav, M.; Gabai, R.; Willner, I. *Langmuir* **2000**, *16*, 8789.
(54) Wang, D.; Li, Y. *J. Am. Chem. Soc.* **2010**, *132*, 6280.
(55) Liu, X.; Wang, A.; Yang, X.; Zhang, T.; Mou, C.-Y.; Su, D.-S.; Li, J. *Chem. Mater.* **2009**, *21*, 410.
(56) Yan, J.-M.; Zhang, X.-B.; Akita, T.; Haruta, M.; Xu, Q. *J. Am. Chem. Soc.* **2010**, *132*, 5326.
(57) Abadias, G.; Gilles, B.; Marty, A. *Appl. Surf. Sci.* **2001**, *177*, 273.
(58) Trant, A. G.; Jones, T. E.; Gustafson, J.; Noakes, T. C. Q.; Bailey, P.; Baddeley, C. J. *Surf. Sci.* **2009**, *603*, 571.
(59) Molenbroek, A. M.; Norskov, J. K.; Clausen, B. S. *J. Phys. Chem. B* **2001**, *105*, 5450.
(60) Bauer, J. C.; Mullins, D.; Li, M.; Wu, Z.; Payzant, E. A.; Overbury, S. H.; Dai, S. *Phys. Chem. Chem. Phys.* **2011**, *13*, 2571.
(61) Wang, Z.-j.; Fu, Q.; Wang, Z.; Bao, X. *Surf. Sci.* **2012**, *606*, 1313.
(62) Lin, S. D.; Bollinger, M.; Vannice, M. A. *Catal. Lett.* **1993**, *17*, 245.
(63) Iizuka, Y.; Tode, T.; Takao, T.; Yatsu, K.; Takeuchi, T.; Tsubota, S.; Haruta, M. *J. Catal.* **1999**, *187*, 50.
(64) Li, L.; Wang, A.; Qiao, B.; Lin, J.; Huang, Y.; Wang, X.; Zhang, T. *J. Catal.* **2013**, *299*, 90.
(65) Aguilar-Guerrero, V.; Gates, B. C. *Catal. Lett.* **2009**, *130*, 108.
(66) Zhou, Z.; Flytzani-Stephanopoulos, M.; Saltsburg, H. *J. Catal.* **2011**, *280*, 255.
(67) Yan, T.; Redman, D. W.; Yu, W.-Y.; Flaherty, D. W.; Rodriguez, J. A.; Mullins, C. B. *J. Catal.* **2012**, *294*, 216.
(68) Sun, D. P.; Gu, X. K.; Ouyang, R. H.; Su, H. Y.; Fu, Q.; Bao, X. H.; Li, W. X. *J. Phys. Chem. C* **2012**, *116*, 7491.
(69) Zhou, Z.; Kooi, S.; Flytzani-Stephanopoulos, M.; Saltsburg, H. *Adv. Funct. Mater.* **2008**, *18*, 2801.
(70) Guczi, L.; Pászti, Z.; Frey, K.; Beck, A.; Pető, G.; Daróczy, C. S. *Top. Catal.* **2006**, *39*, 137.
(71) Yin, H.; Ma, Z.; Chi, M.; Dai, S. *Catal. Today* **2011**, *160*, 87.
(72) Zhao, G.; Hu, H.; Deng, M.; Lu, Y. *Chem. Commun.* **2011**, *47*, 9642.
(73) Herzing, A. A.; Kiely, C. J.; Carley, A. F.; Landon, P.; Hutchings, G. J. *Science* **2008**, *321*, 1331.
(74) Deng, W.; Carpenter, C.; Yi, N.; Flytzani-Stephanopoulos, M. *Top. Catal.* **2007**, *44*, 199.
(75) Guo, X.; Fu, Q.; Ning, Y. X.; Wei, M. M.; Li, M. R.; Zhang, S.; Jiang, Z.; Bao, X. H. *J. Am. Chem. Soc.* **2012**, *134*, 12350.